Proceedings of the ASME 2020 Conference on Smart Materials, Adaptive Structures and Intelligent Systems
SMASIS 2020
September 14-16, 2020, Irvine, CA, USA

SMASIS2020-2444

CHARACTERIZATION OF A MULTIFUNCTIONAL BIOINSPIRED PIEZOELECTRIC SWIMMER AND ENERGY HARVESTER

Yu-Cheng Wang, Eetu Kohtanen, and Alper Erturk*
G.W. Woodruff School of Mechanical Engineering
Georgia Institute of Technology
Atlanta, Georgia 30332

ABSTRACT

Fiber-based flexible piezoelectric composites with interdigitated electrodes, namely Macro-Fiber Composite (MFC) structures, strike a balance between the deformation and actuation force capabilities for effective underwater bio-inspired locomotion. These materials are also suitable for vibration-based energy harvesting toward enabling self-powered electronic components. In this work, we design, fabricate, and experimentally characterize an MFC-based bio-inspired swimmer - energy harvester platform. Following in vacuo and in air frequency response experiments, the proposed piezoelectric robotic fish platform is tested and characterized under water for its swimming performance both in free locomotion (in a large water tank) and also in a closed-loop water channel under imposed flow. In addition to swimming speed characterization under resonant actuation, hydrodynamic thrust resultant in both quiescent water and under imposed flow are quantified experimentally. We show that the proposed design easily produces thrust levels on the order of biological fish with similar dimensions. Overall it produces thrust levels higher than other smart material-based designs (such as soft material-based concepts), while offering geometric scalability and silent operation unlike large scale robotic fish platforms that use conventional and bulky actuators. The performance of this untethered swimmer platform in piezoelectric energy harvesting is also quantified by underwater base excitation experiments in a quiescent water and via vortex induced-vibration (VIV) experiments under imposed flow in a water channel. Following basic resistor sweep experiments in underwater base excitation experiments, VIV tests are conducted for cylindrical bluff body configurations of different diameters and distances from the leading edge of the energy harvesting tail portion. The resulting concept and design can find use for underwater swimmer and sensor applications such as ecological monitoring, among others.

INTRODUCTION

Bio-inspired fish-like underwater swimmers offer a viable approach for a range of applications such as ecological studies, underwater exploration and deep ocean mapping [1]. Different approaches to fish-like robot design have emerged naturally as novel ways to improve certain performance characteristics of the swimmers are sought. The thrust generation mechanism is perhaps the most consequential design differentiator. Most swimmers use motors coupled with intricate mechanisms for propulsion [2–8]. This design typically attains a high swimming speed, but falls short on other desirable characteristics. Motor-powered fish tend to be larger than most biological fish. They are also noisy, which may be disruptive for ecological studies.

Smart material-based thrust generation offers a quiet and compact alternative to motor-driven fish. Several different smart materials have been employed. Shape memory alloys (SMA) [9–11] provide an actuation mechanism driven by temperature change. The time-dependent temperature variation needs to be large enough to cause phase changes within the material for high

*Corresponding author, email: alper.erturk@gatech.edu

actuation loads. Of course, the need for large temperature change makes SMA-based robotic fish poor candidates for autonomous studies where the control of temperature may be limited. Ionic-polymer metal composite (IPMC) [12–16] is perhaps the most popular smart material for underwater swimmers. IPMC is attractive for robotic fish because its actuation mechanism bears a resemblance to muscle contraction. Actuation in IPMC is achieved using an imbalance of ions within a polymer membrane to create local swelling and shrinking of the material. IPMC designs employ high deflections, but their actuation force is low, resulting in slow swimming speeds.

Piezoelectric materials provide another avenue for smart material-based autonomous swimmers, offering high actuation forces and control, while requiring only electrical voltage stimulation IPMCs [17]. Cen and Erturk [18] demonstrated the use of a piezoelectric macro-fiber composite (MFC) bimorph as the tail of a bio-inspired robotic fish. Their design involved a bluff body to house the electronics and a small active tail, resulting in a relatively slow piezoelectric underwater swimmer.

Recently, another underwater swimmer with an MFC bimorph tail was demonstrated [19]. The design includes a passive caudal fin to improve the actuation potential of the active tail. The swimming speed was found to exceed that of other smart material-based swimmers. In this work, the same swimmer and its next generation version are thoroughly characterized in terms of its swimming speed and thrust generation. Working towards truly autonomous systems and to support wireless sensors nodes, additional analyses showcase the energy harvesting performance of the swimmer due to vortex-induced vibration and underwater base excitation.

DESIGN AND MANUFACTURING

The design of the robotic fish in this work was inspired by carangiform locomotion exhibited by fish like trout. The thrust-generating components of the design involve actively controllable bimorph piezoelectric patches coupled with a passive caudal fin. MFC was chosen as the patch material as it can exhibit significantly larger deflections compared to many alternative piezoelectric materials like ceramic-based piezoelectric composites, resulting in higher thrust generation capability. Additionally, the MFC is attached to a passive caudal fin which further aids propulsion. The thrust-generating components of the fish involve approximately one third of the torso, remaining true to the carangiform inspiration. The rest of the fish torso was divided into two additional parts, the nose and the body, where some space is reserved for electronics such as a battery and a voltage amplifier. Since the energy harvesting capabilities due to vortex-induced vibration are of interest, the fish body was also designed to fit the energy harvesting platform configuration. In the following subsections, the design and manufacture of the fish are thoroughly discussed.

CAD Modeling

The body shape of a trout is hydrodynamically similar to the NACA 63A016 airfoil [20]. The fish design here involves a 3.2 mm (1/8”) thick hollow shell in the form of this NACA airfoil for housing the electronics. Figure 1 depicts a drawing of the robotic fish with reference sketches to illustrate the trout-like form of the design. The shell consists of three parts (the nose, the body, and the tail) and spans a total length of 30.5 cm (12”). To secure the nose and the body together, four holes were added to the nose part for the attachment of 4-40 bolts and nuts. To waterproof the design, both the nose and the body feature a shallow 1.6 mm (1/16”) ridge to hold a gasket. Furthermore, the tail part features an embedded silicone flange that compresses between two acrylic plates, providing a watertight seal as the tail is fastened onto the body with screws. The screws serve the additional function of providing electrical connection to the piezoelectric bimorph within the tail. The electronics inside of the body are housed on two U-channels that allow for seamless sliding in and out of the body.

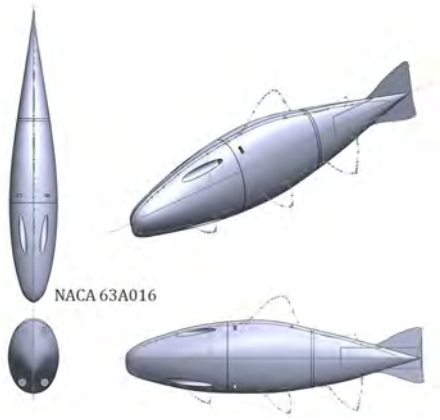

FIGURE 1. SolidWorks drawings of the robotic fish

Manufacturing Process

PLA was used to 3D print the nose and the body. The layer lines on the exterior surfaces were smoothed out with a thin coat of JB-Weld. To secure the nose and the body together, four 4-40 nuts were placed inside the body and fixed in place with JB-Weld. The nose was designed with four grooves such that bolts can freely slide in and engage with the nuts. The nose-body joint was waterproofed with a gasket made by spraying mold release on the nose and filling in the groove between the nose and the body with silicone (GE Silicone II). The two parts were then fastened together, and the silicone was allowed to cure overnight. Afterwards, the nose and the body were detached, leaving the

gasket attached to the fish body. The nose and body were also sanded smooth, spray painted with a primer coat, a coat of Plasti-dip, and two layers of a clear coat.

The flexible tail was made by vacuum bonding a pair of MFCs (M8528-P1) onto a 0.25 mm (0.010") thick PVC substrate using a high shear strength epoxy (3M DP-460). The flexible tapered section of the tail was made using a four-part mold. First the bimorph and the acrylic plate were placed inside the mold, after which a silicone mixture (Ecoflex 00-10 and glass microspheres to increase buoyancy) was poured in. This silicone tail was pressed into the body for water-proofing, and fastened with four 4-40 screws and a laser cut acrylic flange placed on the inside of the body. An electrical connection from the MFC tail to the electronics inside the body was established by attaching soldered wires from the MFC electrodes onto 4-40 nuts used for fastening the body and the tail. From the nuts, a soldered connection was created to a 4x2 female header strip placed near the nose-body joint for easy connection to the MFC. The wiring on the header strip was created such that flipping the orientation of the associated male header pins would only flip the direction of the fish without effecting its overall performance. Figure 2 shows the fully constructed fish, as well as its electronics base, which will be described next.

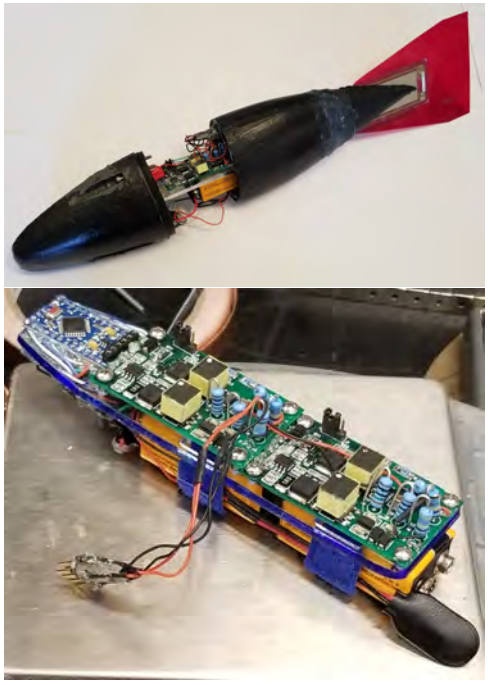

FIGURE 2. Fully constructed robotic fish (top) and its electronics (bottom)

The electronics were soldered together into a single compact unit and mounted onto a 3.2 mm (1/8") thick laser cut acrylic base, letting the unit easily slide in and out of the fish body. The electronics unit is controlled by an Arduino Pro Mini using a mobile app (Blynk) connection established via a Bluetooth module (HC-06). With the app, commands can be sent to the microcontroller via virtual pins, allowing for precise control of the DC voltage, voltage amplitude, and the actuation frequency sent to each of the MFCs in the bimorph tail. The signals to the microcontroller were converted to an analog voltage output by sending a PWM signal through a low-pass filter into two high voltage amplifiers (AMD2012-CE3 from Smart Material Corp.) also attached to the electronics unit. The high voltage amplifiers have a bilinear amplification scheme which maps to the -500V to 1500V voltage range of the MFCs. The high voltage amplifiers can be disabled with a digital on-off safety switch included in the software. Additionally, the electronics unit also contains a 5V and 12V voltage regulator, two 9V batteries, and a master kill switch. While the nose-body-tail gaskets and coats waterproof the electronics by themselves, further caution was exercised by placing the electronics unit inside a ziplock bag. Finally, neodymium magnets were placed below the batteries for added mass to move down the center of gravity for stable swimming and to decrease the buoyancy of the fish.

EXPERIMENTAL PROCEDURES AND RESULTS

Swimming Characterization

Swimming velocity of the robotic fish was analyzed under different water conditions (still and flowing). First, the robotic fish was placed at the end of a small water tank of length 99 cm (39") shown in Figure 3. It was then allowed to reach a steady position, after which the MFCs were actuated using a 500V DC and 1000V amplitude sinusoid, with the two sides of the bimorph actuated out of phase at a varied frequency. Four red trackers were distributed along the length of the fish for velocity extraction via color-based object tracking. The trackers can be clearly seen in top-down video of the fish—composite image containing two video frames is shown on the right of Figure 3. Note the measuring tape on top of the composite image used for converting the length from pixels.

MATLAB was used as the image processing an object tracking tool. The videos were imported and the length scale was converted from pixels to meters. The displacement for each of the four trackers relative to their distinct starting locations was tracked in time and differentiated to obtain the velocity. The top two charts of Figure 4 show the average displacement and velocity normalized to number of body lengths (30.5 cm / 12") per second across all trackers. Note that the displacement has a discontinuity slightly before six seconds. Here, the fish hit the back wall of the water tank and came to rest. The velocity here increases approximately linearly, and presumably would have in-

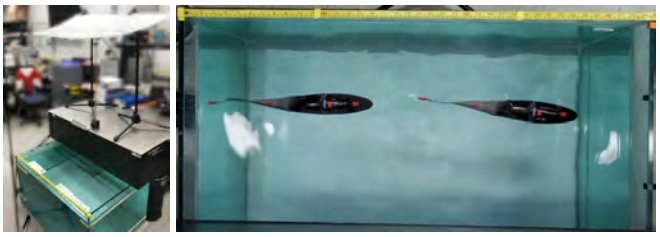

FIGURE 3. Experimental setup depicting the water tank and an overhead camera setup with a light diffuser (top) and two time instance from the video of the swimming robotic fish (bottom)

creased further with a longer water tank.

To capture the maximum velocity of the fish, more experiments were conducted in a larger water tank, where the fish was readily able to reach its full swimming potential in still water. Video was recorded from the side due to the setup of the water tank facility. In this case, the fish was allowed to reach its full steady state swimming speed prior to entering the video frame—a composite image of the swimmer is shown in Figure 5. The known body length of the fish was used for length conversion from pixels. The displacement and the velocity are then extracted using the same object tracking process. Sample displacement and velocity data are shown in the bottom of Figure 4. The maximum instantaneous speed was 0.84 BL/s, and the average speed from the entire video is 0.55 BL/s.

Next, the swimming performance of the fish under imposed flow was measured. An ELD Inc. water tunnel with test section dimensions of 15.24 cm x 15.24 cm x 45.72 cm and a maximum flow speed of 1 m/s was used as the testing apparatus. To measure the electrical power consumptions, the robotic fish was tethered to a pair of high voltage amplifiers (Trek PA05039). The fish was placed inside the test section and the flow speed was incremented until the actuated fish remained stationary within the section. Fishing line kept the fish centered along the spanwise direction. An actuation frequency sweep was performed to measure the tail's underwater resonance frequency. In Figure 6, the steady state swimming speed is plotted against the tail actuation frequency. The resonance is observed at 5.4 Hz with a maximum swimming speed of 0.71 BL/s. From the voltage and current data, the average electrical power for the two high voltage amplifiers used for powering the fish was 0.25 W.

Note that the maximum swimming speed under imposed flow (0.71 BL/s) is lower than the maximum speed in quiescent water (0.84 BL/s). This is because the fish was close to the sides of the water channel due to its limited span. The swimming speed for both quiescent water and imposed flow cases could be improved if it were possible to place the fish farther from the free surface to avoid undesired surface effects.

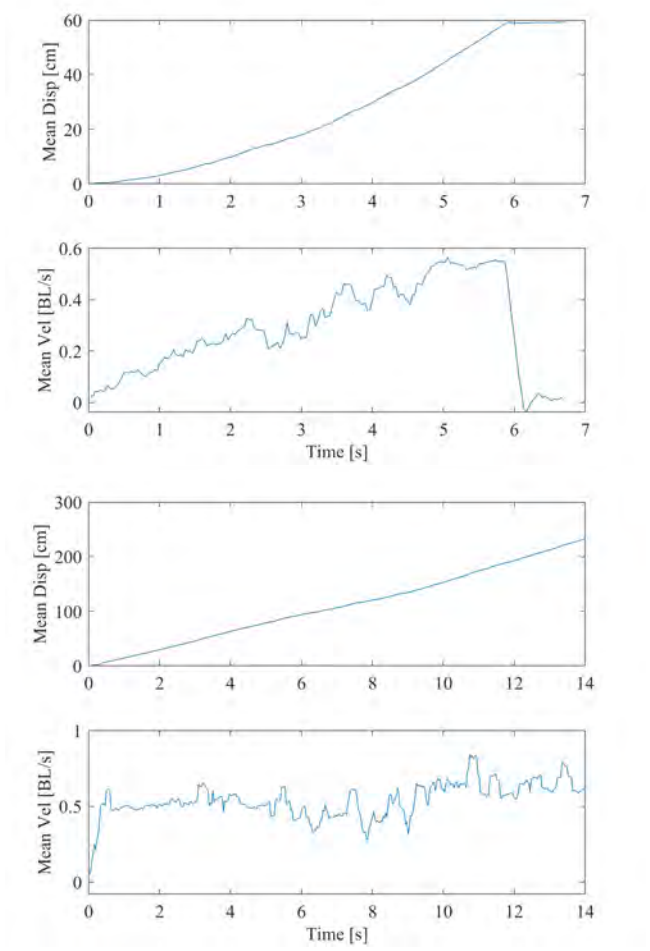

FIGURE 4. Sample displacement and normalized speed versus time in a small tank with limited space demonstrating acceleration from rest (top), and in a large water tank (bottom) where the fish was allowed to reach steady state velocity before entering the video frame

FIGURE 5. Multiple time instances from video of the robotic fish swimming in a large water tank with still water

Thrust Characterization

We also investigate the thrust generation for our second-generation fin design. It differs from the first-generation design in that an additional bimorph MFC is attached onto the PVC substrate to form a double bimorph configuration as shown in

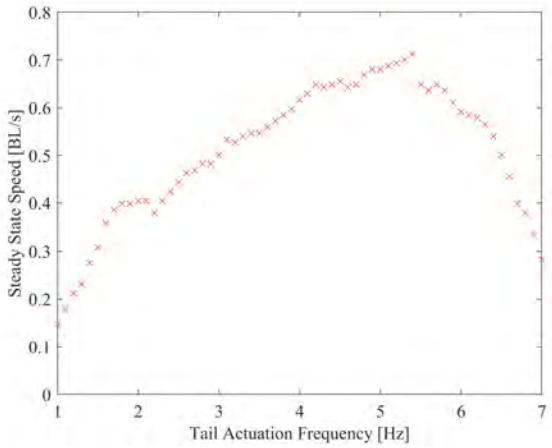

FIGURE 6. Water tunnel used for experiments with imposed flow (left) and the steady state speed of the robotic fish versus tail actuation frequency as measured in the water tunnel (right)

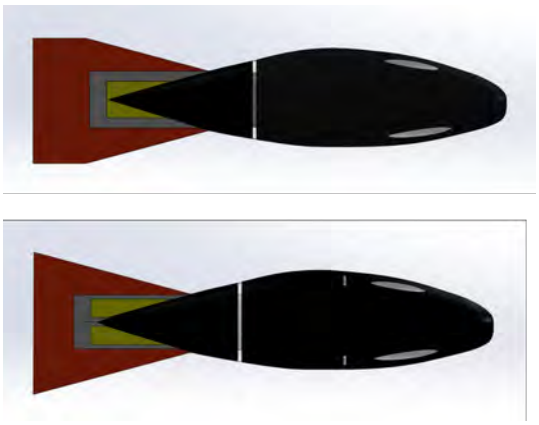

FIGURE 7. (top) First-generation design, (bottom) Second-generation design

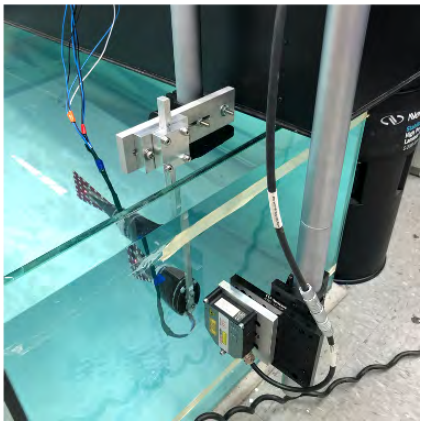

FIGURE 8. Experimental setup for underwater thrust measurement

Fig. 7, allowing for selective excitation of modes other than the first bending. This experiment was performed under the similar setup as in energy harvesting case where the body of the fish as well as the caudal fin portion were fixed onto a 254 mm 25.4 mm 6.35 mm aluminum cantilever and immersed in a water tank as shown in Fig. 8. The force measurement was based on the bar deflection due to hydrodynamics forces generated by the fin. First, it was necessary to conduct the calibration process for the cantilever such that the force-deflection information can be extracted and converted to underwater thrust measurement. A detailed experimental procedure can be found in [21].

Fig. 9 shows the frequency response of thrust generation. Three distinct vibration modes were observed, with each mode corresponding to a local peak thrust value. The third mode is of particular interest because it attains the highest thrust levels. This is in good agreement with the literature, where the thrust performance of a caudal fin has been previously demonstrated to be greatly improved when both flapping and cupping motion appear simultaneously.

Vortex-Induced Vibration Energy Harvesting

Next, the energy harvesting performance is quantified. While in conventional vibration energy harvesting systems the structure is typically excited by means of a mechanical shaker, here the excitation is provided by vortices shed from an upstream bluff body, resulting in vortex-induced vibrations. In the energy harvesting platform, all the MFCs are connected in parallel. First, tests were conducted to verify that there is no charge cancellation occurring during the flapping motion of the tail when subjected to the imposed water flow. The time series data showed that there is no observable phase difference between the MFCs on the same side of the fin within the target flow speed range.

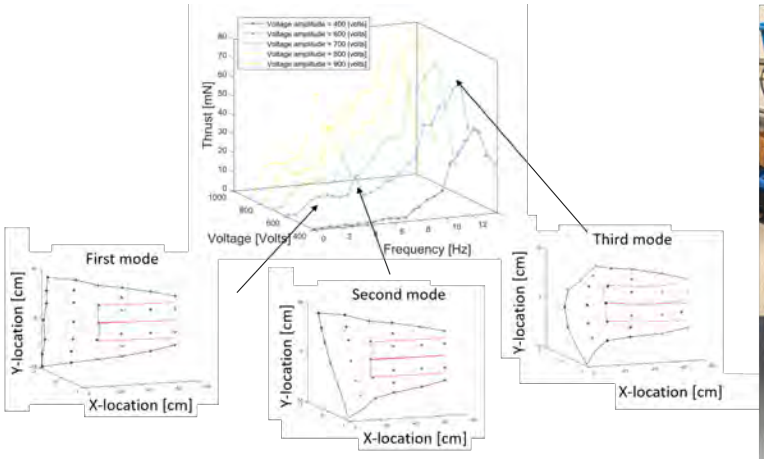

FIGURE 9. Underwater thrust generation under various actuation voltage levels and mode shapes associated with three different actuation frequencies

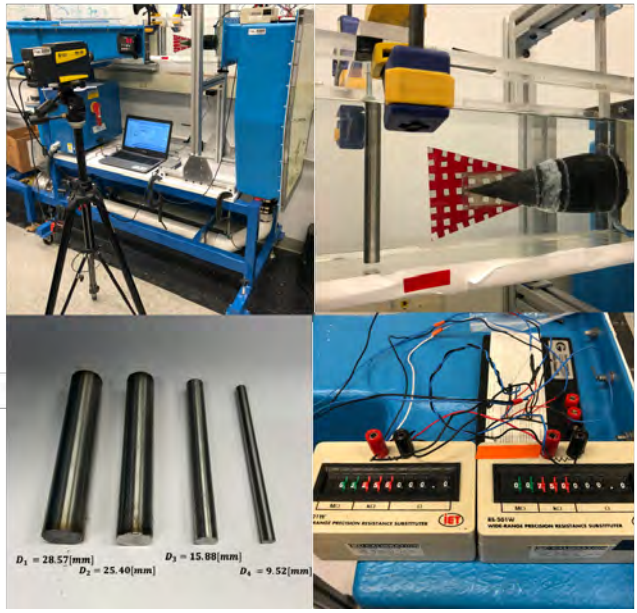

FIGURE 10. Experimental setup for vortex-induced vibration energy harvesting system

However, for higher flow speeds there is an obvious twisting motion of the fin that leads to a significant drop in the output voltage across the external resistance because of charge cancellation.

The swimmer, oriented with its tail facing the flow, is attached to a fixed rod such that the caudal fin is in the middle of the test section as seen in Fig. 10. To attach the swimmer, its nose was removed and the exposed surface waterproofed with a custom silicone gasket. In addition, adjustable resistance boxes were used as the external loading. A Laser Doppler Vibrometer () was used to measure the velocity of the fin. An NI 9223 data acquisition device was used for recording the time series of both voltages across the resistance boxes as well as the velocity measurement of the fin, from which the frequency information is extracted in postprocessing.

Based on the empirical formula, the approximate optimal impedance can be evaluated by $R_{opt} = \frac{1}{\omega C_p}$ where C_p is the effective capacitance value of two bimorph MFCs under a parallel connection. The capacitance values were measured before and after underwater immersion to assure the experiments were conducted in good standing, and only minor differences were observed.

First, the effects of the distance between the center of the bluff body and the leading edge of the fin in power generation were investigated. The fin was positioned at different locations along and across the wake. The piezoelectric voltage across the resistance load of $R = 3M\Omega$ was measured, and a cylinder with a diameter of 25.4 millimeters was aligned with the centerline of the testing section. The 3D plot of the RMS electrical power versus distance and flow speed is shown in Fig. 11. The maximum power was observed when the fin was positioned along the centerline of the wake and the leading edge of the fin is two and half times the diameter of the bluff body. The power extracted from the piezoelectric fin decayed when the position of the fin moved away in either direction. This can be explained by the intensity of vortex shedding which exhibited viscous dissipation and growth in their sizes while moving downstream.

Next, a resistance sweep for two different sizes of diameter cylinder was also measured. In this study, circular cylinders with a diameter of 25.40*mm* and 15.88*mm* were tested, and the position of the cylinder was fixed to the distance of two and half times of the cylinder size as we observed from the previous test. Resistive load of $3M\Omega$ was chosen to be the center value as suggested by the optimal resistance expression, and various different values of resistive loads were tested with an increment of 0.5 in a log scale. The extracted RMS electrical power from the fin was obtained and shown in Fig. 12.

The last parametric study in this work focused on the size effects where cylinders with a diameter of 28.57mm, 25.40mm, 15.88mm, and 9.52mm are studied. The experiment in this study was performed under the fixed position configuration where the distance between the center of the cylinder and the leading edge of the fin kept a constant value of 60mm. However, since the peak value obtained from the target flow speed range differs for each cylinder, the selection of resistive load is unique to each cylinder case and determined again by the approximate optimal resistance expression. Fig. 13 shows the results of the study on size effects with respect to the imposed flow speed (top) and frequency (bottom). It is noted that the vortex shedding fre-

quency can be approximately evaluated by an empirical expression $f = S_t \frac{U}{L}$ where U is the imposed flow speed, L is the characteristic length of the bluff body, and S_t is the Strouhal number which is a dimensionless parameter that describes oscillating flow mechanisms. In addition, the Strouhal number is also a function of the Reynolds number. However, for Reynolds number in the range of 300 to 20000, the Strouhal number can be considered a constant value of 0.2. The results in this work are obtained within this Reynolds number range, and the vortex shedding behavior from each cylinder closely follows the $S_t = 0.2$ line in Fig. 14 .

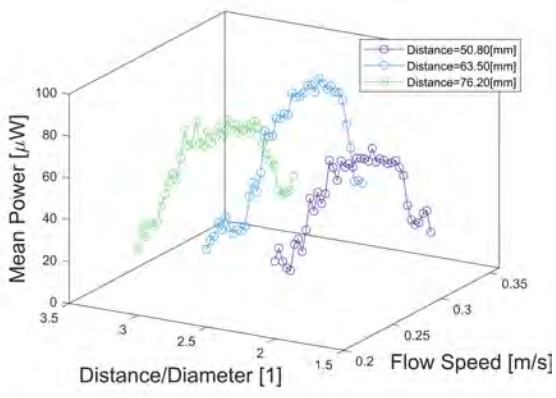

FIGURE 11. Study on distance effects of circular bluff body

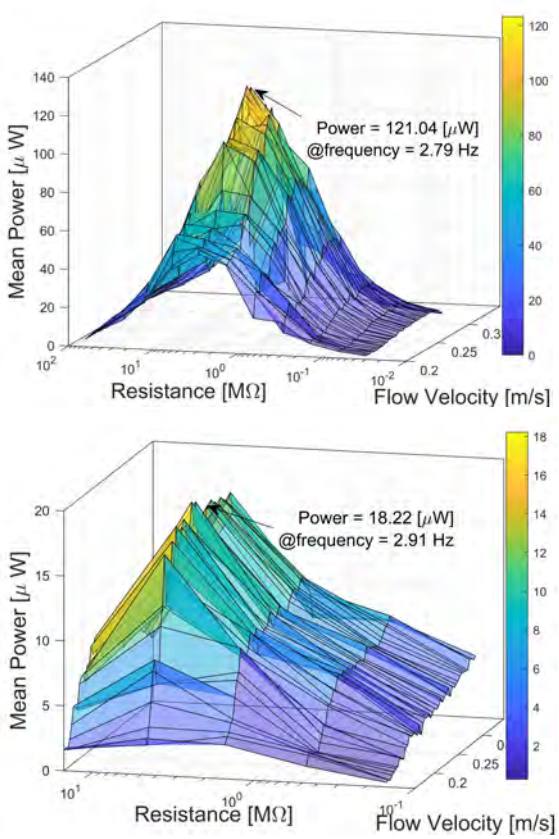

FIGURE 12. Resistance sweep center with the optimal resistance at resistive load of $R = 3M\Omega$ (top)case of diameter =25.40mm (bottom)case of diameter = 15.88mm

CONCLUSIONS

A bio-inspired fish-like robotic swimmer and energy harvesting platform was investigated in this work. The piezoelectric macro-fiber composite was used as the thrust generating mechanism for robotic fish design and manufacturing. The performance of the robotic fish was characterized in both quiescent water and under imposed flow, where the maximum speed was measured as 0.84 BL/s and 0.71 BL/s, respectively. This robotic fish platform is faster than other smart material based, bio-inspired fish-like robots found in literature due to the high actuation authority of piezoelectric materials and the streamlined design. The actuation itself is simple in nature, only requiring a sinusoidal input to each of the MFCs. In the experiments where the flow was imposed, the robotic fish was close to the sidewalls of the water tunnel, resulting in slightly lower swimming speed. On the other hand, in the vortex-induced energy harvesting platform, three parametric studies including the location of the bluff body, the size of the bluff body, and resistance sweep were performed. The optimal distance was observed to be the distance of two and half times of the cylinder size. A maximum electrical power extracted from the piezoelectric caudal fin was found to be 121.04μW in the second generation fin design. Also, the thrust generation characterization for double bimorph fin design was investigated and found to generate a maximum thrust in 80mN. Further efforts will be placed onto the speed characterization and thrust measurement via a multi-axis force transducer to perceive the feasibility of 3D thrust generation fin design.

ACKNOWLEDGMENT

This work was supported by NSF CMMI Award No. 1254262 and CBET Award No. 1705739. The authors also acknowledge contributions of Mr. David Tan for the earlier development of the robotic fish prototype.

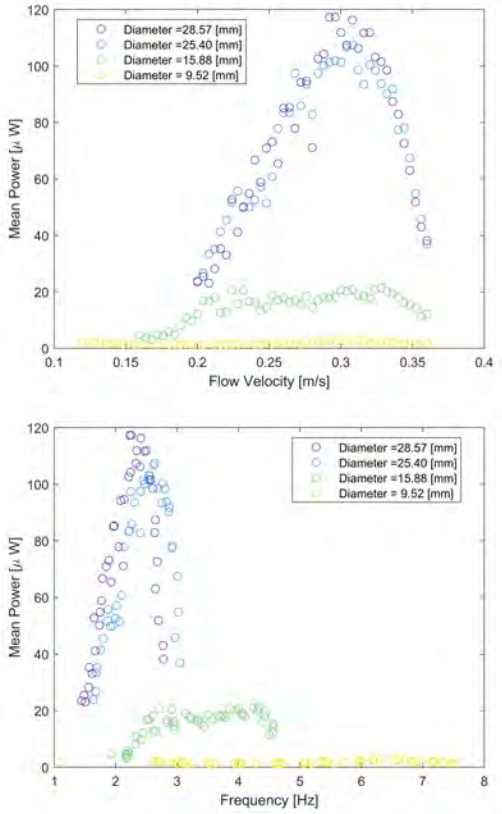

FIGURE 13. Study on the geometric effects for circular bluff body with four difference sizes in diameter (top)the mean power versus flow velocity (bottom)the mean power versus frequency of the tail measured by a LDV

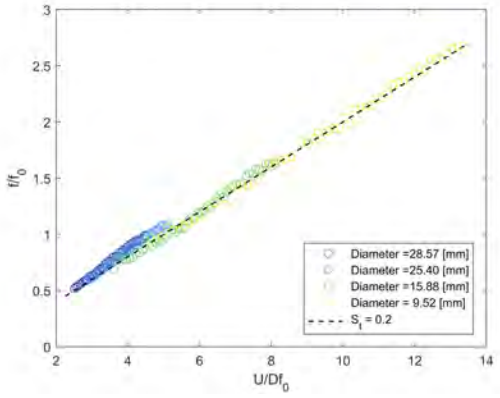

FIGURE 14. Dimensionless analysis for vortex shedding under four cases

REFERENCES

[1] Griffiths, G., 2002. *Technology and Applications of Autonomous Underwater Vehicles*. CRC Press.

[2] Hirata, K., 2000. "Development of experimental fish robot". In Sixth International Symposium on Marine Engineering.

[3] Hu, H., 2006. "Biologically inspired design of autonomous robotic fish at essex". In IEEE SMC UK-RI chapter conference.

[4] Konno, A., Furuya, T., Mizuno, A., Hishinuma, K., Hirata, K., and Kawada, M., 2006. "Development of turtle-like submersible vehicle". *Marine Engineering,* ***41***(SI), pp. 158–163.

[5] Liu, J.-D., and Hu, H., 2006. "Biologically inspired behaviour design for autonomous robotic fish". *International Journal of Automation and Computing,* ***3***(4), pp. 336–347.

[6] Epps, B. P., Valdivia y Alvarado, P., Youcef-Toumi, K., and Techet, A. H., 2009. "Swimming performance of a biomimetic compliant fish-like robot". *Experiments in Fluids,* ***47***(6), pp. 927–939.

[7] Papadopoulos, E., Apostolopoulos, E., and Tsigkourakos, P., 2009. "Design, control, and experimental performance of a teleoperated robotic fish". In 17th Mediterranean Conference on Control and Automation, IEEE, pp. 766–771.

[8] Sitorus, P. E., Nazaruddin, Y. Y., Leksono, E., and Budiyono, A., 2009. "Design and implementation of paired pectoral fins locomotion of labriform fish applied to a fish robot". *Journal of Bionic Engineering,* ***6***(1), pp. 37–45.

[9] Shinjo, N., and Swain, G. W., 2004. "Use of a shape memory alloy for the design of an oscillatory propulsion system". *IEEE Journal of Oceanic Engineering,* ***29***(3), pp. 750–755.

[10] Wang, Z., Hang, G., Wang, Y., Li, J., and Du, W., 2008. "Embedded SMA wire actuated biomimetic fin: a module for biomimetic underwater propulsion". *Smart Materials and Structures,* ***17***(2), p. 025039.

[11] Rossi, C., Colorado, J., Coral, W., and Barrientos, A., 2011. "Bending continuous structures with SMAs: a novel robotic fish design". *Bioinspiration & Biomimetics,* ***6***(4), p. 045005.

[12] Guo, S., Fukuda, T., and Asaka, K., 2003. "A new type of fish-like underwater microrobot". *IEEE/ASME Transactions on Mechatronics,* ***8***(1), pp. 136–141.

[13] Tan, X., Kim, D., Usher, N., Laboy, D., Jackson, J., Kapetanovic, A., Rapai, J., Sabadus, B., and Zhou, X., 2006. "An autonomous robotic fish for mobile sensing". In IEEE/RSJ International Conference on Intelligent Robots and Systems, IEEE, pp. 5424–5429.

[14] Ye, X., Su, Y., Guo, S., and Wang, L., 2008. "Design and realization of a remote control centimeter-scale robotic fish". In IEEE/ASME International Conference on Advanced Intelligent Mechatronics, IEEE, pp. 25–30.

[15] Brunetto, P., Fortuna, L., Graziani, S., and Strazzeri, S., 2008. "A model of ionic polymer–metal composite actuators in underwater operations". *Smart materials and Structures,* ***17***(2), p. 025029.

[16] Aureli, M., Kopman, V., and Porfiri, M., 2010. "Free-locomotion of underwater vehicles actuated by ionic polymer metal composites". *IEEE/ASME Transactions on Mechatronics,* ***15***(4), pp. 603–614.

[17] Heo, S., Wiguna, T., Park, H. C., and Goo, N. S., 2007. "Effect of an artificial caudal fin on the performance of a biomimetic fish robot propelled by piezoelectric actuators". *Journal of Bionic Engineering,* ***4***(3), pp. 151–158.

[18] Cen, L., and Erturk, A., 2013. "Bio-inspired aquatic robotics by untethered piezohydroelastic actuation". *Bioinspiration & Biomimetics,* ***8***(1), p. 016006.

[19] Tan, D., Le Dault, Y.-A., and Erturk, A., 2019. "Characterization of a bio-inspired piezoelectric swimmer in a quiescent water and under imposed flow". In Active and Passive Smart Structures and Integrated Systems XIII, Vol. 10967, International Society for Optics and Photonics.

[20] Azuma, A., 2006. *The Biokinetics of Flying and Swimming*, second ed. American Institute of Aeronautics and Astronautics, Inc., Reston, VA.

[21] Erturk, A., and Delporte, G., 2011. "Underwater thrust and power generation using flexible piezoelectric composites: an experimental investigation toward self-powered swimmer-sensor platforms". *Smart materials and Structures,* ***20***(12), p. 125013.